JOURNAL OF Materials CHEMISTRY

Highly oriented 3D-hexagonal silica thin films produced with cetyltrimethylammonium bromide

D. Grosso,*[a] A. R. Balkenende,[b] P. A. Albouy,[c] M. Lavergne,[d] L. Mazerolles[e] and F. Babonneau[a]

[a]*Laboratoire Chimie de la Matière Condensée, Université Pierre et Marie Curie, 4 Place Jussieu, 75252 Paris Cedex 05, France. E-mail: grosso@ccr.jussieu.fr*
[b]*Philips Research Laboratories, Prof. Holstlaan 4, 5656 AA Eindhoven, Netherlands*
[c]*Laboratoire de Physique des Solides, Université Paris-Sud, 91405 Orsay Cedex, France*
[d]*Laboratoire de Réactivité de Surface, Université Pierre et Marie Curie, 4 Place Jussieu, 75252 Paris Cedex 05, France*
[e]*CECM-CNRS, 15 rue G. Urbain, 94407 Vitry sur Seine Cedex, France*

Received 19th April 2000, Accepted 23rd June 2000
Published on the Web 31st July 2000

Mesoporous silica thin films have been produced by sol–gel chemistry in the presence of cetyltrimethylammonium bromide (CTAB) template. The films were deposited on silicon or glass substrates by dip-coating and underwent different treatments to eliminate the CTAB and create porosity. As-prepared and treated coatings exhibit good optical quality. Their structures were fully characterised by transmission electron microscopy (TEM) performed on film cross-sections and by X-ray diffraction (XRD) in θ–2θ scan mode, as well as in transmission mode using two different scattering geometries. The films exhibit large and homogeneous domains organised in a 3D-hexagonal ($P6_3/mmc$) structure with the c axis normal to the surface throughout their whole thickness. Numerical analysis of the TEM pictures confirms the space group deduced from the XRD measurements. To our knowledge, these are the first reported thin films obtained by dip-coating in the presence of CTAB which show such extended and highly mono-oriented 3D-hexagonal ($P6_3/mmc$) domains. The film thickness, porosity and refractive index were evaluated by ellipsometry for the various treated films.

1 Introduction

Since the discovery of the family of MCM mesoporous materials by researchers from the Mobil Corporation,[1,2] such nanostructured inorganic materials have been studied for a variety of applications in the areas of separation, catalysis, encapsulation, chemical sensing, low-dielectric coatings, and optical thin films.[3–7] The most common method used to produce porous ordered bulk materials consists of adding an aqueous solution of surfactant to a solution of inorganic precursors (often silicates). A self-assembly process usually occurs between the organic and inorganic entities, leading to the precipitation of oxide particles containing organised cavities of homogeneous dimensions filled with the organic templating phase. The removal of this organic phase leads to mesoporous oxide powders. Different mesostructures can be obtained by varying the synthetic conditions.

The design of mesoporous thin films as optical anti-reflective or low-dielectric coatings is now of great interest, since the shape, size and organisation of the pores, in addition to the porosity, can be controlled. Many studies have been reported, employing a variety of techniques to produce mesoporous films, *e.g.* by a growing process at water/air[8–10] or water/mica[11,12] interfaces, by dip-coating[13–18] or by spin-coating.[19–21] The preparation of high optical quality thin films by dip-coating requires a low silicate precursor condensation rate and homogeneous wetting of the selected substrates. The initial solution thus contains a low quantity of water and is highly diluted in a solvent that has good wettability properties with the substrates. Once the liquid film is deposited, mesophase formation occurs within the film *via* evaporation-induced self-assembly.[18] The solvent first departs from the film, inducing an increase in the water content. As a result, several mechanisms, mainly governed by the rate of solvent evaporation, compete during a very short period of time (*ca.* 30 s): auto-assembly of organic and inorganic species, organisation of entities and polycondensation of the network. In order to obtain homogeneous structured mesoporous films, it is necessary that formation of the mesophase occurs before the polycondensation of the inorganic species is too advanced along the drying process, which will cause an increase in the wet film viscosity, preventing film organisation. On the other hand, the preferential evaporation of the solvent induces an increase in the water concentration with time. If the system is not condensed enough when the water content becomes largely predominant, the sol on the surface tends to form localised drops due to the low surface tension of water with the substrate. The film viscosity must, therefore, be high enough to withstand this non-wetting phenomenon. As a result, too high a degree of condensation of the inorganic species present in the initial sol leads to non-organised films, and too low a degree of condensation leads to non-homogeneous films. Moreover, this process is complicated by the fact that the evaporation of solvent and water during the drying process occurs at the air/film interface, inducing gradients of concentrations in the film thickness. The kinetics of self-assembly and organisation are, therefore, expected to be different when comparing the area close to both interfaces and the central part of the coating.[13] As a result of all these simultaneous reactions, it is difficult to fully understand the formation of such thin films.

In the present work, the sol was prepared *via* acidic hydrolysis–condensation of tetraethoxysilane (TEOS) in the presence of cetyltrimethylammonium bromide (CTAB: $C_{16}H_{33}N(CH_3)_3Br$) as the structure-directing agent. Several treatments were used to remove the template from the pores. As such coatings may be designed to be components of devices

DOI: 10.1039/b003178j

that may not support high temperatures, efforts have been made to try some low-temperature two-step treatments. The film structure has been characterised by X-ray diffraction analyses in transmission mode, with two different orientations of the coating with respect to the incident X-ray beam. This simple analysis, never applied before on such systems, allows us to deduce the structure and the possible structural anisotropy induced by the dip-coating method (preferential orientation of the organised domains with respect to the substrate surface). TEM images of film cross-sections and XRD patterns in θ–2θ conventional scan mode were also collected from as-prepared and treated films. TEM images were analysed by Fourier transformation and displayed patterns that correspond to those obtained by XRD in transmission mode. The optical characteristics of the films were studied by ellipsometry.

2 Experimental

2.1 Preparation of coatings

A prehydrolysed solution was prepared by refluxing for 1 h an ethanolic solution containing TEOS, deionised water and hydrochloric acid in the following molar ratio: 1 TEOS : 3 EtOH : 5×10^{-5} HCl : 1 H_2O. Then, CTAB was dissolved in ethanol and added to the prehydrolysed solution together with an additional amount of water and HCl. Typically, the final molar ratio was 1 TEOS : 20 EtOH : 0.004 HCl : 5 H_2O : 0.10 CTAB. The final solution was then stirred for 48 h at room temperature before deposition. The templated films were produced by dip-coating on glass substrates or thin (100) silicon wafers at a constant withdrawal rate of 3.1 mm s^{-1}. These were then allowed to dry at room temperature for several hours. In order to stiffen the silica network and remove the surfactant phase, various treatments were applied to the films (Table 1). Film D25 is the as-prepared film dried at 25 °C. Film C350 was slowly heated from 160 to 350 °C in air (1 °C min^{-1} ramp, followed by 5 h at 350 °C). Film C160-SOX was heat-treated in air for 1 h at 160 °C and the surfactant removed by soxhlet extraction in hot ethanol for 5 h. Film NH-SOX was exposed to an NH_3-saturated atmosphere for 45 min before being subjected to soxhlet extraction in hot ethanol for 5 h. Analysis of the composition by Rutherford back scattering (RBS) and FTIR spectroscopy did not show any residual carbon, bromine or nitrogen after these treatments.

2.2 Characterisation techniques

The structures of the as-prepared and treated coatings were deduced by XRD, using Cu-Kα radiation from a rotating anode. θ–2θ diffractograms of films deposited on glass substrates were recorded with a conventional goniometer (acquisition time: 1 s per 0.005° step). Diffraction patterns were recorded on image plates in transmission mode using a self-built diffractometer and two different geometries, with the X-ray beam incidence angles fixed at 0 or 90° with respect to the film surface. The distance between the film and the image plate was 500 mm and the acquisition time ranged from 2 to 10 h. For these latter analyses, 8 μm thick silicon wafers were chosen as substrates to reduce absorption and background effects.

Table 1 Conditions employed for production of the various treated films

Film samples	Treatments
D25	As-prepared film dried at 25 °C
C350	Film calcined at 350 °C
C160-SOX	Heat treatment at 160 °C, then soxhlet extraction in ethanol
NH-SOX	Exposure to NH_3 atmosphere, then soxhlet extraction in ethanol

Micrographs of the C160-SOX films were obtained with a transmission electron microscope (TEM) JEOL 100 CX II apparatus. Cross-sections of films deposited on Si substrates were produced by diamond-cutting and were deposited on a carbon-coated copper grid. For comparison, pieces of films were scratched from the substrate and also analysed by TEM. Numerical treatment by Fourier transformation of the TEM images was performed after digitisation of the experimental images. This treatment led to the corresponding local numerical diffraction patterns and to images reconstructed from the Bragg spots of the diffraction (Bragg filtering). Ellipsometry measurements on coatings deposited on glass plates were carried out with a variable angle spectroscopic ellipsometer (Woollam VASE instrument). Optical properties were deduced by fitting the obtained ellipsometric ψ and Δ optical quantities, measured at 10 nm intervals between 400 and 1400 nm for incidence angles of 53, 56 and 59°. The models used for fitting consisted of a glass substrate with a porous SiO_2 film on top. The thickness and the refractive index of the top layer were the only fitted parameters, assuming a certain volume of voids in the silica (using a Bruggeman effective medium approximation).

3 Results

3.1 θ–2θ XRD experiments

The as-prepared and treated coatings exhibit good optical quality. Their thickness varies from 70 to 500 nm, depending on the deposition rate. XRD spectra of the as-prepared and treated coatings, recorded in the θ–2θ scan mode, are shown in Fig. 1. They all exhibit intense and narrow Bragg diffraction peaks in addition to their first harmonics, suggesting the presence of large, highly organised domains with a single ordered structure. It was observed that these diffraction peaks are shifted to larger values of 2θ upon coating treatment, suggesting a contraction of the structure in a direction perpendicular to the substrate (Table 2). The corresponding d-spacings are: 39 Å for D25 coatings, 35 Å for C160-SOX coatings, 31 Å for NH-SOX coatings and 30 Å for C350 coatings. The highest contraction (23%) is observed after calcination at 350 °C, while the lowest (10%) is obtained for the C160-SOX films. The intensity of the diffraction peak does not vary significantly with the treatments. On the other hand, the

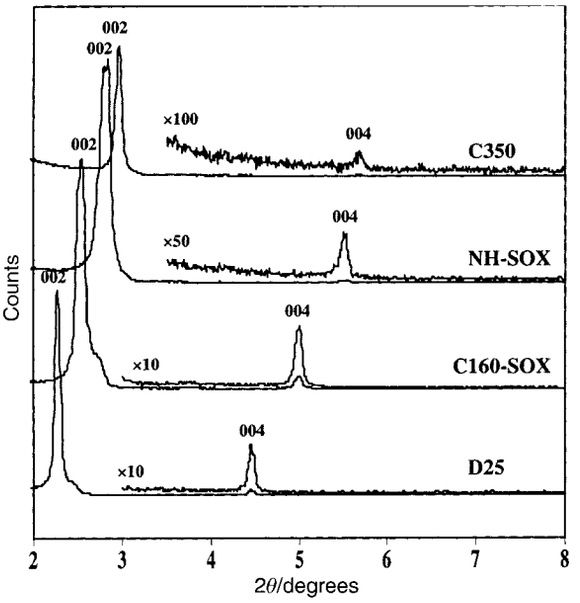

Fig. 1 X-Ray diffraction patterns recorded in θ–2θ scan mode using Cu-Kα radiation, for the as-prepared and treated films deposited on glass substrates.

Table 2 Refractive indices (n), porosity (P) and film contractions ($\Delta h/h_0$) deduced from ellipsometry measurements and XRD in transmission and θ–2θ modes

Film	Refractive index, n	Porosity, P (vol.%)	Contraction (%)		
			$\Delta h/h_0$	XRD (trans.)	XRD (θ–2θ)
D25	1.47	—	—	—	—
C160-SOX	1.31	32	8	15	10
NH-SOX	1.35	22	17	20	20
C350	1.31	32	22	26	23

line width, characteristic of the extent of organisation, increases slightly. This is indicative of a degree of structural degradation.

3.2 XRD experiments in transmission mode

The presence of only one series of diffraction peaks in Fig. 1 suggests that the organised domains are mono-oriented, preventing identification of the 3D-structure of the film, a result which has been achieved in previously published studies as a result of lower degrees of orientation.[13,15] This prompted us to record XRD patterns in transmission mode with an image plate system coupled to two different scattering geometries[22] (Fig. 2). The angle (θ) of the X-ray beam with respect to the film surface was set at 0 (Fig. 2b) or 90° (Fig. 2a). Fig. 2b ($\theta = 0°$) was collected with the as-prepared D25 sample and shows well-defined diffraction spots which can be assigned to a 3D-hexagonal $P6_3/mmc$ structure, with the C_6 axis normal to the substrate surface. The conditions of possible diffraction are verified (hhl: $l = 2n$). The cell parameters were calculated to be $a = 54 \pm 1.0$ and $c = 75 \pm 1$ Å. The first intense and the second less intense diffraction rings in Fig. 2a ($\theta = 90°$) were attributed to (100) and (110), respectively. The distance obtained, $d(100) = 46.5 \pm 0.5$ Å, is in good agreement with the a value calculated from Fig. 2b [$a = 2/\sqrt{3} \times d(100) = 53.7$ Å]. The fact that the rings are continuous suggests that the $\{hk0\}$ planes, which are normal to the surface, have random orientations. This implies that no anisotropy was induced by the dip-coating withdrawal procedure. The diffraction peaks recorded in the θ–2θ scan mode (Fig. 1) can now be assigned to (002) and (004), leading to $c = 78$ Å, in agreement with the value previously calculated from Fig. 2b. The organisation of pores in the present 3D mesoporous coatings can thus be assimilated to an hexagonal cell where pores are located at coordinates ($x = 0$, $y = 0$, $z = 0$) and ($x = 1/3$, $y = 2/3$, $z = 1/2$). The c axis direction is normal to the substrate and a can be found in any direction in the {00l} plane.

The XRD patterns obtained in transmission mode with $\theta = 0°$ for the various treated samples are shown in Fig. 3. They correspond to a 3D-hexagonal ($P6_3/mmc$) structure with a similar a value of 54 ± 1 Å but a contracted c value, as observed in the θ–2θ mode XRD studies (Fig. 1). Here, the c values obtained are 78 Å for D25, 66 Å for C160-SOX, 62 Å for NH-SOX and 58 Å for C350. The corresponding contractions with respect to the initial D25 dry film are 15, 20 and 26% respectively (Table 2). Since a is unchanged and c decreases after treatment, the contraction of the network applies only in the direction normal to the substrate (c axis).[23,24]

3.3 TEM investigation

A TEM image of a section of the C160-SOX film is shown in Fig. 4a, with the modulus of the Fourier transform corresponding to the local diffraction pattern, and the reconstructed image by inverse Fourier transformation in Fig. 4b. It can be seen that the pores are well organised into large domains throughout the thickness of the entire film. The Fourier transformed pattern corresponds to the diffraction pattern in the [0,1,0] zone axis, revealing that the cutting follows a (−210) plane. The filtered image clearly confirms the contracted hexagonal arrangement. The presence of channel-like features close to the air/film interface suggests that the pores may be interconnected. A piece of C160-SOX treated film scratched from the glass substrate has also been analysed by TEM for comparison. The perfect hexagonal disposition of pores can clearly be seen on both the real and reconstructed images (Fig. 5a and b). Hence, this view corresponds to the (001) plane, coplanar to the surface. Periodic distances measured on such images are not reported here but were slightly smaller than those obtained by XRD. This may be due to focussing effects and network alteration often observed with TEM analysis.

3.4 Ellipsometry results

The refractive indices (n), porosities (P) and contractions in the film thickness ($\Delta h/h_0$) deduced from ellipsometry are reported in Table 2. The porosity deduced from the refractive index of a porous film depends on the shape and orientation of the pores. In the particular case of mesoporous films where the pores are

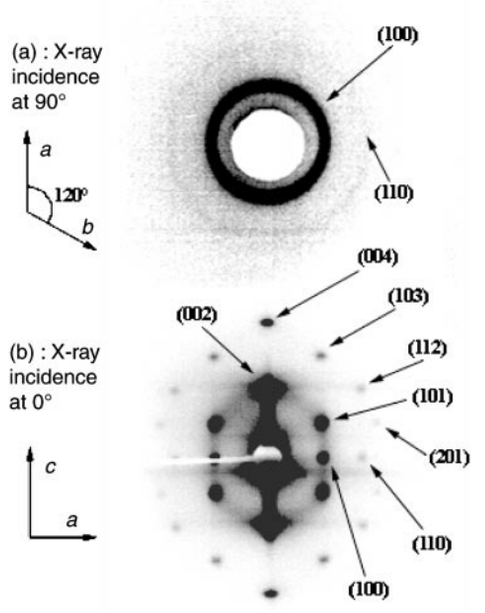

Fig. 2 X-Ray diffraction patterns obtained on image plates in transmission mode for the as-prepared and dried D25 film deposited on a (100) Si substrate. The X-ray beam was normal (90°) to the surface for (a) and parallel (0°) to the surface for (b).

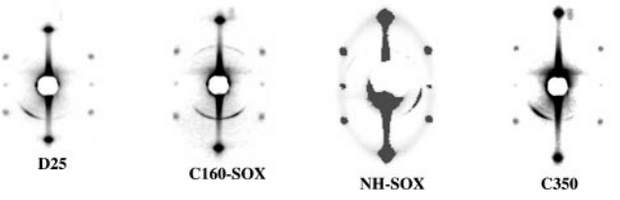

Fig. 3 X-Ray diffraction patterns obtained on image plates in transmission mode for the as-prepared and treated films deposited on Si substrates. The X-ray beam was parallel (0°) to the surface.

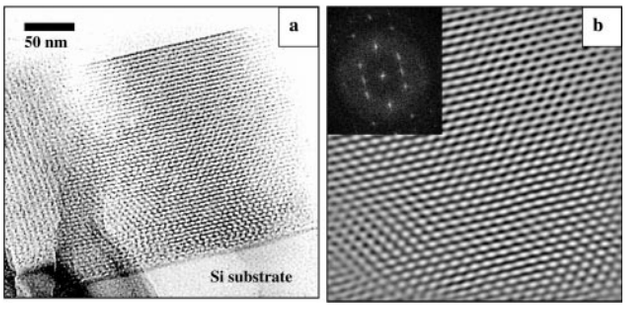

Fig. 4 Cross-sectional TEM image of C160-SOX treated film deposited on a Si substrate (a), modulus of Fourier transform and reconstructed image (b).

cylinders preferentially aligned with the surface, a birefringence is observed and the transverse refractive index is lower than the longitudinal one. Taking into account only the transverse refractive index leads to an under-estimation of the porosity by ellipsometry. In the present case, the pores are either spherical or ellipsoidal with homogeneous distribution within the film. The porosity deduced here should be close to the real pore volume fraction. Refractive indices ranging from 1.31 to 1.35 lead to porous volumes from 22 to 32%.

4 Discussion

To our knowledge, the films described in the present paper are the first dip-coated films prepared with CTAB which exhibit a single type of highly mono-oriented $P6_3/mmc$ structured domains. They extend throughout the whole thickness, with the c axis normal to the substrate. Mesoporous films with 3D-hexagonal domains have already been obtained; Tolbert *et al.*[12] prepared highly oriented films with the same $P6_3/mmc$ space group by using a less-common double-headed quaternary amine surfactant and an interfacial silica–surfactant self-assembly process. The $P6_3/mmc$ space group has also been found by Zhao *et al.*[14] for dip-coated films using lower molecular weight alkyl(ethylene oxide) non-ionic surfactants. Also employing dip-coating, but with CTAB as surfactant, Lu *et al.*[13] reported the formation of cubic and 3D-hexagonal films. However, their results differ from ours; the structures of the as-deposited films were found to be either lamellar or 1D-hexagonal, depending on the CTAB concentration. One of the lamellar phases then transformed into a new phase composed of cubic and 3D-hexagonal phases upon calcination. These observations were obtained from conventional θ–2θ XRD profiles (as in the work of Zhao *et al.*), and this was possible only because of a distribution of orientations for the hexagonal or cubic domains. No space group was given, and the cell parameters of the 3D-hexagonal phase were different from ours ($a=79.1$ and $c=75.6$ Å).

As already reported by Tolbert *et al.*,[12] a way to describe this $P6_3/mmc$ structure is to consider a packing of spherical or ellipsoidal micelles. Indeed, this phase is unusual for lyotropic systems, and has been reported for the first time recently for the $C_{12}EO_8$–water binary system.[25] For silicate powdered materials, this structure has been obtained using divalent quaternary ammonium surfactants[26,27] but never, to our knowledge, using CTAB. This example demonstrates, as already pointed out by Lu *et al.*, that film mesostructures that have no bulk counterparts can be generated.[13]

In a true 3D-hexagonal compact structure based on spherical objects, $c/a=\sqrt{(8/3)}=1.63$, and this value was observed for the bulk $P6_3/mmc$ silicate–surfactant samples prepared with divalent quaternary ammonium surfactants.[27] In our case, for the as-prepared D25 films, $c/a=1.44$. One explanation for this difference could be that, assuming the micelles to be spherical, a true compact 3D-hexagonal structure might have been formed by the packing of the micelles at one point in the solvent evaporation process, during the film formation. But further evaporation–condensation and drying of the film may have induced the contraction, leading to the observed contracted 3D-hexagonal lattice. A second possible explanation for this compact structure distortion may be due to the non-spherical shape of the micelles, as any object of any shape can, in principle, pack in a hexagonal unit cell.

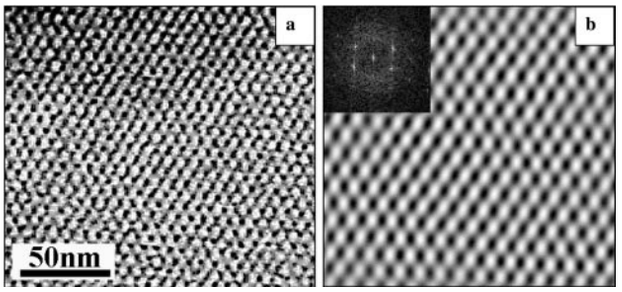

Fig. 5 TEM image of a piece of C160-SOX treated film scratched from the substrate (a), modulus of Fourier transform and reconstructed image (b).

Several treatments have been applied to remove the surfactant, in order to retain the highest degree of organisation and create the largest pore volume. The common treatment is a one-step calcination (350 °C), but for certain applications, the temperatures needed for such treatment may be too high. We have therefore applied lower temperature treatments which involve two steps: the first leads to stiffening of the silicate network, either by low-temperature (160 °C) treatment or by exposure to an ammonia atmosphere. The surfactant is then removed by soxhlet extraction. For each treatment, the $P6_3/mmc$ structure is preserved, with a decrease in the c value, while a remains unchanged. This shows an additional contraction of the film with an amplitude depending on the post-deposition treatment. As the shrinkage of the structure applies only in the direction normal to the surface, the changes in film thickness are similar to the contractions deduced from XRD along the c direction (Table 2). As expected, calcination at 350 °C leads to the highest film contraction ($24\pm2\%$), but, surprisingly, to the highest porosity (32 vol.%). In comparison, the C160-SOX film is characterised by the same porosity, but also by a much lower contraction ($11\pm4\%$). This could be explained by the fact that the degree of condensation of the network is expected to be higher after calcination at 350 °C than for the other two-step treatments. The silica network walls are thus certainly thinner, compensating for the pore volume fraction lost by the contraction. Consequently, the one-step calcination treatment at 350 °C seems to be the best suited to obtaining a condensed porous network. But if a low-temperature treatment is required, then the two-step treatment involving heat-treatment at 160 °C, followed by a soxhlet extraction of the surfactant, seems quite appropriate.

5 Conclusion

The procedure described here allows the preparation of 3D-hexagonal, $P6_3/mmc$, silica mesoporous films with excellent optical quality. Several treatments have been applied in order to remove the surfactant under mild conditions, while retaining a high degree of organisation for the network and creating a large pore volume. The structural characterisation of the films was performed by 2D-XRD in transmission mode using two scattering geometries and was completed by TEM observation of film cross-sections. The combination of these techniques leads to a good description of the phase symmetry, $P6_3/mmc$, which has not, as yet, been reported for thin films prepared with CTAB. Although the details of the pore structure are not yet known, it is reasonable to expect a 3D network of

interconnected pores, which may be of particular interest for applications in the field of membranes or sensors.

Acknowledgements

The authors would like to acknowledge financial support by Philips Research.

References

1 J. S. Beck, J. C. Vartuli, W. J. Roth, M. E. Leonovicz, C. T. Kresge, K. D. Shimtt, C. T-W. Chu, D. H. Olson, E. W. Sheppard, S. B. McCullen, J. B. Higgins and J. L. Schlenker, *J. Am. Chem. Soc.*, 1992, **114**, 10834.
2 J. C. Vartuli, K. D. Schmitt, C. T. Kresge, W. J. Roth, S. B. McCullen, S. D. Hellring, J. S. Beck, J. L. Schlenker, D. H. Olson and E. W. Sheppard, *Chem. Mater.*, 1994, **6**, 2317.
3 N. K. Raman, M. T. Anderson and C. J. Brinker, *Chem. Mater.*, 1996, **8**, 1682.
4 C. J. Brinker, *Curr. Opin. Colloid Interface Sci.*, 1998, **3**, 166.
5 U. Ciesla and F. Schuth, *Microporous Mesoporous Mater.*, 1999, **27**, 131.
6 J. Y. Ying, C. P. Mehnert and M. S. Wong, *Angew. Chem., Int. Ed.*, 1999, **38**, 56.
7 T. J. Barton, L. M. Bull, W. G. Klemperer, D. A. Loy, B. McEnaney, M. Misono, P. A. Monson, G. Pez, G. W. Scherer, J. C. Vartuli and O. M. Yaghi, *Chem. Mater.*, 1999, **11**, 2633.
8 H. Yang, N. Coombs, I. Sokolov and G. A. Ozin, *Nature*, 1996, **381**, 549.
9 A. S. Brown, S. A. Holt, T. Dam, M. Trau and J. W. White, *Langmuir*, 1997, **13**, 6363.
10 H. Yang, N. Coombs and G. A. Ozin, *J. Mater. Chem.*, 1998, **8**, 1205.
11 H. Yang, A. Kuperman, N. Coombs, S. Mamiche-Afara and G. A. Ozin, *Nature*, 1996, **379**, 703.
12 S. H. Tolbert, T. E. Shaffer, J. Feng, P. K. Hansman and G. D. Stucky, *Chem. Mater.*, 1997, **9**, 1962.
13 Y. Lu, R. Ganguli, C. A. Drewien, M. T. Anderson, C. J. Brinker, W. Gong, Y. Guo, H. Soyez, B. Dunn, M. H. Huang and J. I. Zink, *Nature*, 1997, **389**, 364.
14 D. Zhao, P. Yang, N. Melosh, B. F. Chmelka and G. D. Stucky, *Adv. Mater.*, 1998, **10**, 1380.
15 D. Zhao, P. Yang, D. I. Margolese, B. F. Chmelka and G. S. Stucky, *Chem. Commun.*, 1998, 2499.
16 D. A. Doshi, N. Husing, H. Fan, A. J. Hurd and J. C. Brinker, *Mater. Res. Soc. Symp. Proc.*, 1999, **576**, 263.
17 M. Klotz, A. Ayral, C. Guizard and L. Cot, *J. Mater. Chem.*, 2000, **10**, 663.
18 C. J. Brinker, Y. Lu, A. Sellinger and H. Fan, *Adv. Mater.*, 1999, **11**, 579.
19 J. E. Martin, M. T. Anderson, J. Odinek and P. Newcomer, *Langmuir*, 1997, **13**, 4133.
20 J. M. Berquier, I. Teyssedre and C. Jacquiod, *J. Sol–Gel Sci. Technol.*, 1998, **13**, 739.
21 M. Ogawa, H. Ishikawa and T. Kikuchi, *J. Mater. Chem.*, 1998, **8**, 1783.
22 M. Klotz, P. A. Albouy, A. Ayral, C. Ménager, D. Grosso, A. van der Lee, V. Cabuil, F. Babonneau and C. Guizard, *Chem. Mater.*, 2000, **12**, 1721.
23 D. Kundu, H. S. Zhou and I. Honma, *J. Mater. Sci. Lett.*, 1998, **17**, 2089.
24 D. Grosso, A. R. Balkenende, P. A. Albouy and F. Babonneau, *Stud. Surf. Sci. Catal.*, 2000, **125**, 673.
25 M. Clerc, *J. Phys. II*, 1996, **6**, 961.
26 Q. Huo, R. Leon, P. Petroff and G. D. Stucky, *Science*, 1995, **268**, 1324.
27 Q. Huo, D. I. Margolese and G. D. Stucky, *Chem. Mater.*, 1996, **8**, 1147.